

Performance of An Axial Gas Ionization Detector

S. Adhikari¹, C. Basu¹, C. Samanta^{1,2}, S. S. Brahmachari¹, B.P. Das¹ and P. Basu¹

¹ Saha Institute of Nuclear Physics, 1/AF Bidhan nagar, Kolkata-700064, India.

² Physics Department, Virginia Commonwealth University, Richmond, VA 23284-2000, USA.

Abstract

An axial gas ionization chamber has been fabricated for use as a ΔE detector in heavy ion induced nuclear reactions. Different operating parameters such as gas type, pressure, anode voltage and anode structures have been optimized. The transparency of the anode structure is observed to play an important role in improving the energy resolution of the detector.

Keywords: Gas ionization chamber, axial field, anode structure

1 Introduction

Detection of charged particles provides important information about the reaction mechanisms induced by accelerated heavy ions. For light charged particles (LCPs) such as protons, deuterons, alphas solid-state silicon detectors provide excellent energy, timing and position resolution. Moreover, due to higher density of the detecting medium solid-state silicon detectors offer better opportunity to stop high energy charged particles. The solid-state detectors are also prone to permanent radiation damage and therefore inadequate for heavy ion detection. Common problems with highly ionizing particles for these detectors are pulse height defect and plasma delay. Corrections in the measurement are then required to get correct information about the energy and rise time of the interacting radiations.

In highly ionizing environment, on the other hand, gas detectors offer better options [1]. These detectors permit operation under high current rates and high dose environment and the gas can be recycled to maintain the purity of the detecting medium. Gas detectors for charged particles are primarily of two types: 1) the low pressure multiwire counters which show excellent position and timing resolutions [2] and 2) relatively high pressure ionization or proportional chambers for identification and energy measurement of various heavy ions emitted from a nuclear reaction.

Ionization chambers generally operate at the reduced electric field values of $E/P \sim 1$ to 2 Volts/(cm×Torr) where E is the applied electric field and P is the gas pressure. In a typical design of an ionization chamber [3], a transverse field is applied. This field arrangement proves to be disadvantageous as the associated pulse height becomes a function of position where the incident particle impinges [3]. Although, this problem is solved by the introduction of a Frisch grid to the ionization chamber, in an axial field configuration a Frisch grid is not always useful.

The present work describes the performance of a ΔE ionization chamber working in the axial field configuration. The advantage of using an axial field in a ΔE detector over the more usual transverse field has been discussed in ref [4,5]. Since then there has been no studies or development on this form of gas detector. Extensive studies on the different parameters are sparse in the literature. In this paper we have made a detailed study on the different operating parameters of our detector. The gas pressure, bias voltage and window foil thickness of the chamber have been optimized. Earlier studies [4,5] have given little or no importance to the anode structure on the detector performance. A parallel wire anode structure has been used for the first time to achieve very high transparency and its possible effects on the energy resolution have been addressed.

2 Construction of the detector

Fig.1 shows the construction of the detector used in the present studies. The body of the detector is made of aluminium with an active area of 45×45 mm². The window is an aluminized mylar foil mounted by grease (non out-gassing at pressures of at least 10^{-6} Torr) and held by an O-ring in a brass flange. The window foil is maintained at ground potential by contact with

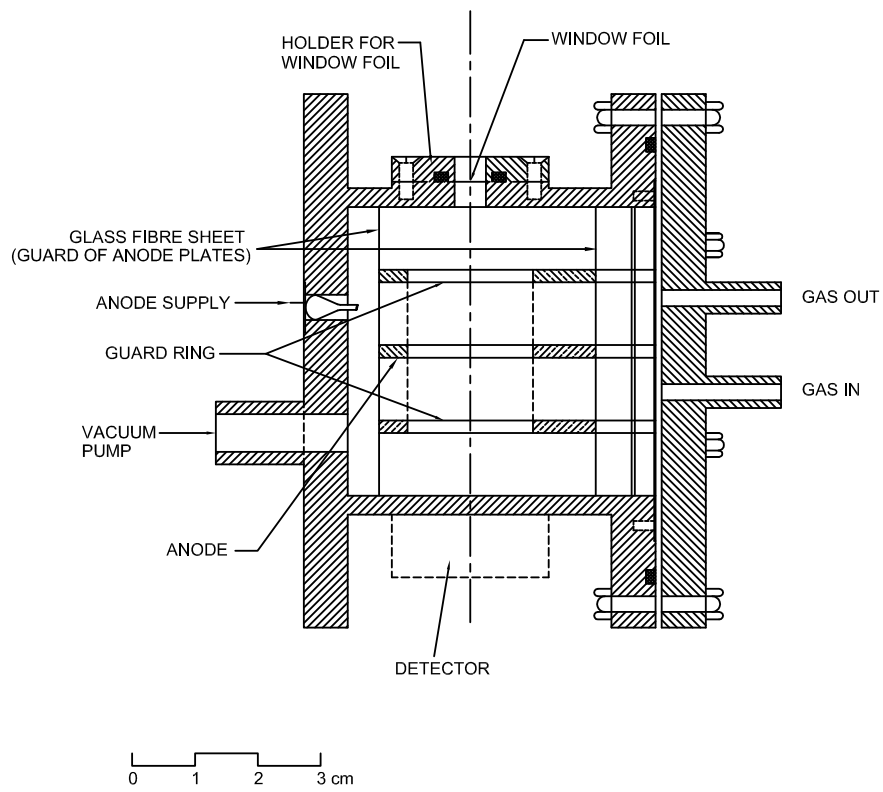


Figure 1: Cross-sectional view of the gas ionization chamber

the screws of the brass flange. The anode structure is located in the middle of the chamber and is mounted on a brass plate of active area $34 \times 34 \text{ mm}^2$ and thickness 2 mm. The plate is provided with a hole of diameter 20 mm. The anode structure is in the form of conducting parallel thin wires or mesh and is mounted on a 1.5 mm thin copper clad G10 board (PCB) of area $30 \times 30 \text{ mm}^2$ with a square hole $20 \times 20 \text{ mm}^2$. The anode assembly is fixed by teflon screws with the central brass plate which is stepped down by the PCB thickness. Different thin wire structures (parallel or crossed) in the anode are used to study its effect on the energy resolution of the detector. In order to maintain the uniformity of the electric field gradient along the incident particle path two additional brass plates are kept at half the anode voltage at 10 mm on either side of the anode. In this way the separation between the plates is made smaller compared to their lengths so that the effect of non-uniform electric field can be ignored. The brass plates are of the same thickness and area as that of the central plate except the hole is kept empty. The 20 mm hole of the guard plates and that of the anode are coaxial with the 5 mm hole of the window. The separation of the first guard plate from the window and the last guard plate to the exit is 9.5 mm. Since the detector will be ultimately used as a ΔE detector the anode is centrally located so that the active volume is extended on both sides of the anode plane.

The voltage to the anode is provided by a kovar seal and the divided voltage to the plates is provided by a breeder (resistive) circuit placed inside the chamber. The plates with applied voltage are isolated from the ground by G10 spacers which cover the inner walls perpendicular to the window and exit side. The body of the detector at the window (including the window foil) and the exit side is at ground. This ensures the field lines along the axis of the chamber. The DC current path and other details of the equivalent circuit describing the resistive gradient is shown in fig.2. Calibrated resistances of value $50 \text{ M}\Omega$ are used to make the resistive gradient. Resistive noise in our case was negligible. The noise level at the preamplifier stage was within 15 mV. One side of the detector is flanged with a viton O-ring for dismantling and testing. The gas inlet-outlet and provision for evacuation of the detector are shown in the figure 1. The system is pumped down to 10^{-3} Torr vacuum and charged with gas at the desired pressure. The detector is now ready to be tested.

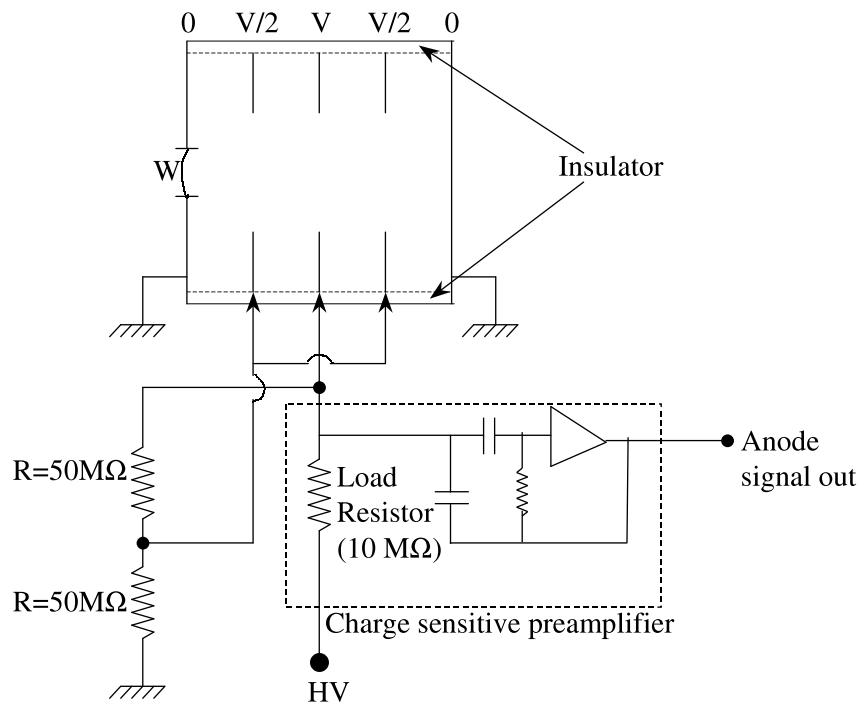


Figure 2: Equivalent circuit describing the resistive gradient and all the ground paths. The details of the preamplifier (Ortec 142IH) circuit are available in the manual.

3 Experiment and discussion of results

The detector performance was tested with a ^{252}Cf α -source. The α -source was collimated to fall on the entrance window which is 5 mm in diameter. The collimation and thickness of the window foil plays an important role on the resolution of the detector. We used a collimation of 1 mm and mylar foils for the window of two different thickness. The detector was filled with gas between 60-600 Torr pressure. Two different gases Ar(90%)-CH₄(10%) and isobutane were used to compare the performance of the chamber in each case. The output of the detector was fed to a charge sensitive preamplifier (ORTEC 142IH) and to a spectroscopy amplifier (ORTEC 672) and finally to a 2K ADC MCA (ORTEC maestro-32). Fig.3 shows the acquired energy-loss spectrum of α particle (84% 6.12 MeV and 15.7% 6.08 MeV) from a collimated ^{252}Cf source of strength 10 μCi .

The different parameters of the detector were optimized to obtain the best possible energy resolution with the collimated alpha spectrum. The energy calibration for the ΔE detector was performed with a ^{241}Am and ^{252}Cf α -particle (5.485 MeV and 6.12 MeV respectively) energy loss and its correlation with the pulse heights. The stopping power of α particles in gases are well accounted by the Bethe-Bloch formula [6]. The mean energy loss (centroids) in the gas and mylar window were thus determined from Bethe-Bloch formula (code SRIM [7]) with the density of gas scaled by the ratio of desired to the normal gas pressure (760 torr). The centroid of the data was obtained by an in-built fitting software of the MCA. This method of energy calibration for ΔE detectors using simulated energy loss have been adopted in studies with solid-state detectors [8]. Two different window foils of thickness 1.5 and 8 μm were examined. For the thicker foil the resolution varied between 9-13% FWHM whereas for the 1.5 μm window the resolution was much better (6-8% FWHM). A possible reason for this is that higher straggling effects in the thicker window foil degrades the resolution of the detector. As the area of the window aperture is small noticeable effect of window deformation due to pressure differences on the either side of the window was not observed. As far as the working gas is concerned, better performance was obtained with isobutane in comparison to Ar(90%)-CH₄(10%). This is depicted in fig. 4(a). A reason for this may be due to the higher energy loss per unit pressure in isobutane [9]. The optimum gas pressure was found to be at 160-200 Torr and bias voltage 200-250 Volts. We show in fig.4 (b) the region of optimum gas pressure

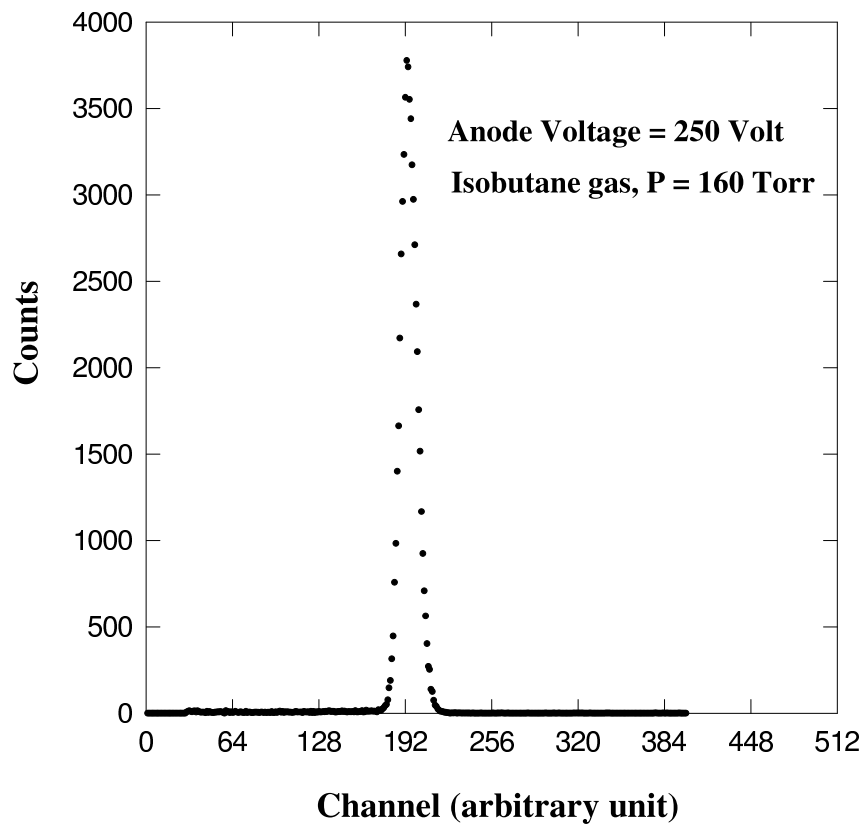


Figure 3: The energy-loss spectrum of α -particle (84% 6.12 MeV and 15.7% 6.08 MeV) from a collimated ^{252}Cf source. The energy resolution is 6.8% FWHM.

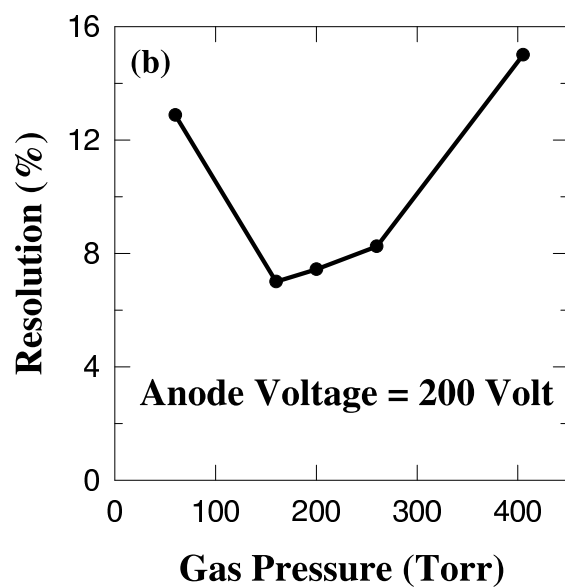
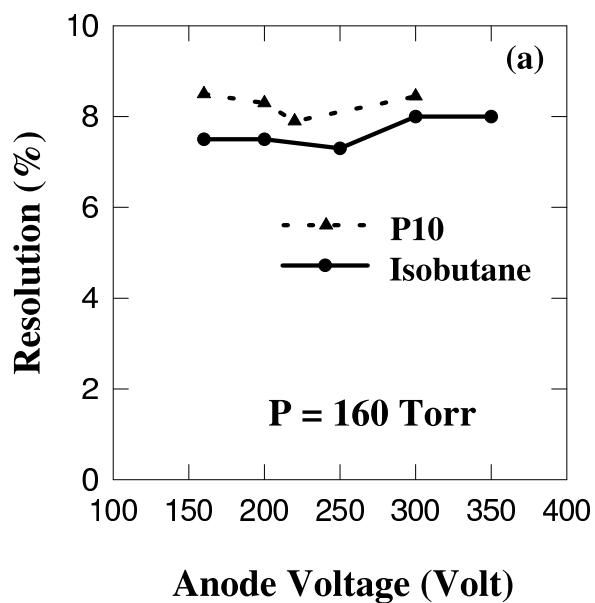


Figure 4: Variation of energy resolution with (a) anode voltage at a fixed gas pressure (160 Torr) for two different types of gas Isobutane and Ar(90%)-CH₄(10%) (P10) and (b) with gas pressure at a fixed anode voltage (200 V).

Table 1: Energy loss and resolution in keV are given at different gas pressures for Isobutane and P10 gases.

Gas Pressure (Torr)	Isobutane		P10	
	Energy Loss (keV)	FWHM(expt) (keV)	Energy Loss (keV)	FWHM(expt) (keV)
60	365.3	47.03	261.3	-
160	973.6	68.15	697.1	55.77
200	1217.6	90.56	871.3	74.06
260	1582.8	130.48	1132.8	107.61
405	2466.0	369.90	1764.4	-

(160-250 torr) at 200 Volts bias. At lower gas pressures (60 - 100 Torr) the recombination effect is overcome earlier though the resolution is poorer than at higher pressures. The statistical fluctuation in the number of electron ion pairs created is larger at lower pressure due to lower energy loss (hence poorer resolution). At higher pressure the resolution is mainly limited due to increased recombination [4,10]. The energy loss of the alpha particle in the gas and FWHM of the observed peak in energy unit is given in table 1 at anode voltage, $V = 200\text{V}$ and shaping time = $3\mu\text{s}$. The operating reduced electric field (E/P) was found to be between 1-2 Volts/(cm \times Torr). A gaussian shaping for optimum signal-to-noise ratio was used and the optimum amplifier shaping time was found to be $3\mu\text{s}$ (charge collection time for our detector is about 400 ns). The resolution degraded at higher and lower shaping time. The detector could handle about 500 counts per second with good resolution.

The effect of the anode structure on the energy resolution has not been addressed by earlier workers [4,5]. In ref [5] an electro-formed nickel mesh was used with high transparency (97%). But no justification was given for choosing such an anode structure. F.H. Read et al [11], have made an extensive computational study about the electrostatic problems involving a mesh sandwiched between plates on either side kept at different voltages. The effect of a mesh made of a) parallel ultra thin round wires and b) crossed round wires have been studied. According to this work, the potential on the mesh is modified depending on the structure and transparency of the mesh.

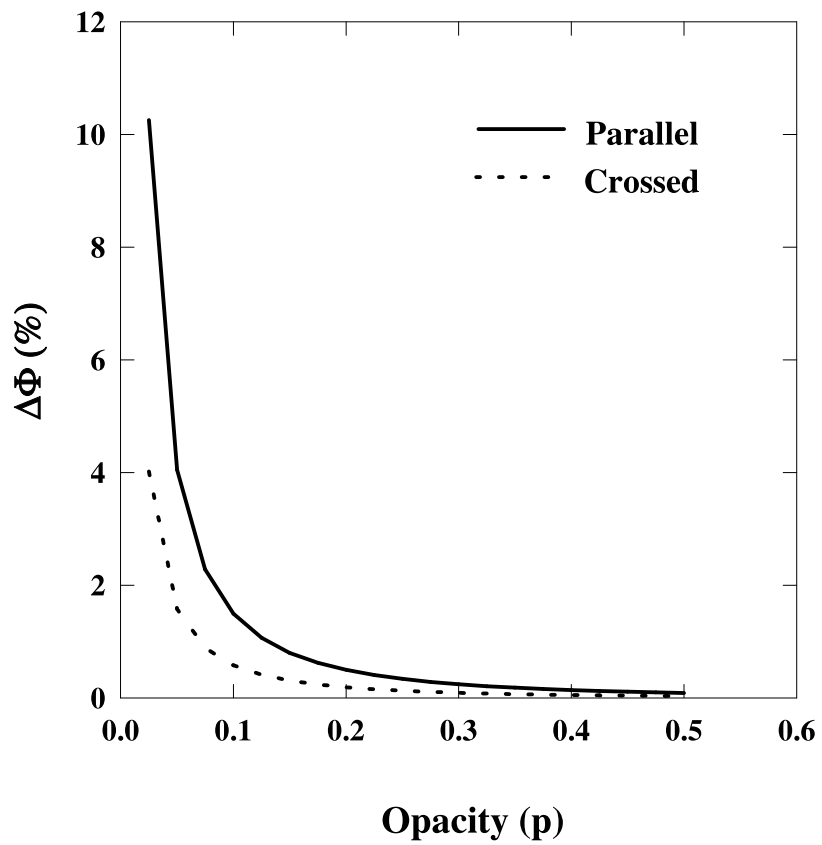


Figure 5: Plot of variation of percentage potential shift per unit field difference ($\Delta\Phi$) with opacity(p) for parallel and crossed wire mesh.

The fluctuation of potential on the mesh (ϕ_m) is defined as

$$\phi_m = \Delta\mathcal{E}\Delta\phi \quad (1)$$

$$\Delta\phi = s\chi_m \quad (2)$$

where $\Delta\mathcal{E}$ is the difference in electric fields on either side of the mesh, $\Delta\phi$ denotes the potential shift per unit field difference, χ_m is a dimensionless parameter that depends on the transparency (opacity) of the mesh and s is the separation between any two adjacent wires in the mesh [11]. The percentage variation of potential shift per unit field difference ($\Delta\phi$ %) for crossed and parallel wires with opacity (p) is displayed in figure 5. It is clearly seen that with very high transparency (small opacity) $\Delta\phi$ is very large and the mean voltage on the mesh will shift considerably even if $\Delta\mathcal{E}$ is small. (For the present electrode configuration the magnitude of the electric field is same but changes sign on either side of the anode.) At the same transparency however this shift is reduced by a factor of 2 in comparison to a mesh of parallel wires (figure 5). This is due to the reduction of the parameter χ_m by this factor in the latter case [11]. It is therefore interesting to study how the fluctuation of potential (if any) and structure of the anode affect the resolution of the detector.

Anode structures made of parallel and crossed ultra thin wires were used in the present ionization detector. For the crossed anode structure an electro-formed Nickel mesh acquired from Precision e-forming, USA with transparency of 89% was used. For this mesh the expected potential shift is only 1% for our detector configuration. The best resolution that obtained with this anode structure was about 7.5% FWHM. The anode structure made of parallel wires was self-fabricated with gold plated platinum wires. The wire diameter was kept $50\mu\text{m}$ and wire spacing 2 mm. The transparency in this case was 97.5%. A resolution of 7.3% FWHM was obtained with this anode structure. Though for the latter anode structure $\Delta\phi$ could be as high as 10% we did not observe any significant effect of this increase on the resolution. Instead the effect of transparency could be seen through the improvement in resolution with increase in transparency. The reason for better resolution for more transparent electrodes is due to the reduced input capacitance of the preamplifier. The opacity of a crossed mesh is roughly twice than that with parallel wires for the same ratio of wire-diameter to wire-spacing. Therefore it is more convenient to work with parallel wires that can be fabricated to very high transparency. In order to test the effect of transparency on resolution we used another anode structure where

the wire diameter was taken to be $12.5 \mu\text{m}$, keeping the wire spacing to be 2mm as before. The transparency for this case was even higher (99.4%). Though the expected potential fluctuation on the wires is very high in this case we found an improvement in resolution, which is found to be within 7.0% FWHM.

In the extreme case of a blank anode i.e. the anode frame made of brass plate with the 20 mm hole at the center was used without any mesh or wires. Here in this case however no improvement of resolution was observed. This structure also required a higher amplifier shaping time ($6 \mu\text{s}$) for the best possible resolution (8%). This is because with the blank hole anode the charge collection is not as efficient as with an anode with conductors in the hole. The use of a highly transparent mesh as anode is therefore suitable for improving the resolution. This can be achieved more easily with parallel arrangement of anode wires rather than with a crossed structure. In all the measurements, fresh gas was used for each different anode structure so that the relative error between any two measurement (due to gas impurity) is negligible.

Performance of the detector for heavy ions were studied by recording the ΔE spectrum of the spontaneous fission fragments from ^{252}Cf . The acquired spectrum is displayed in fig.6. The light (on the right) and heavy fragments (on the left) are observed to be reasonably separated. The optimum anode structure was the one with $12.5\mu\text{m}$ parallel thin wires and gas pressure at 60 Torr. At higher pressures the separation degraded possibly due to increased recombination. The peak to valley ratio was seen to improve with collimation of the source. The fission E spectrum parameters for a solid-state detector described in ref [3] are evaluated for the present detector and depicted in table 2. The ^{252}Cf fission spectrum has been studied in [12] by a gas ΔE chamber where the best peak to valley ratio is 2.8. However, in [12] the source is placed inside the detector volume and the window effect is avoided. In [13] ^{252}Cf spectrum has been measured by a gas E detector and the peak to valley ratio for light and heavy fragments are quoted as 2.25 and 2.07 respectively. These parameters in the present case are thus within reasonable limit. It should be however noted that the intensities of the light and heavy fragments interchange in the recorded ΔE spectrum in comparison to a typical E spectrum of the fission fragments. The heavy fragments (left) have higher intensity than that of the lighter fragments. This is owing to increased energy straggling of the lighter fragment than the heavier one as studied in ref [14]. Similar shift in the heavy and light group has

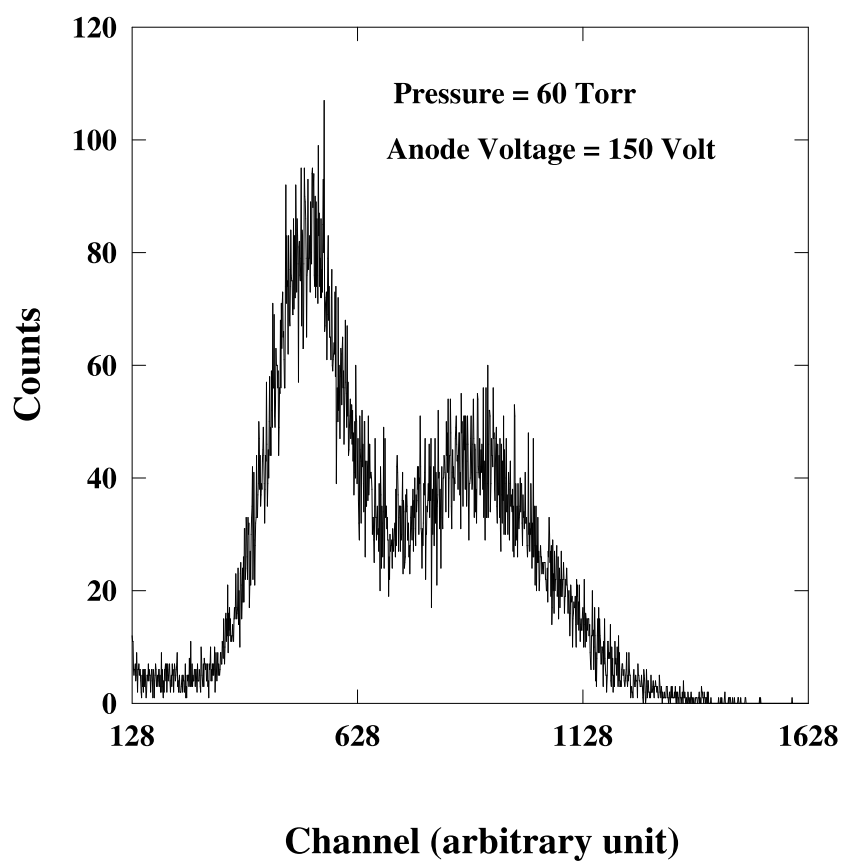


Figure 6: The energy-loss spectrum of spontaneous fission fragments from ^{252}Cf source. The heavy fragments on the left have higher intensities than that of lighter fragments.

Table 2: Parameters of the ^{252}Cf ΔE fission fragment spectrum. The definition of the different parameters are same as in ref [3].

Spectrum Parameter	Values
N_H/N_V	3.8
N_L/N_V	2.2
N_H/N_L	1.7
$\Delta L/(L - H)$	0.3
$\Delta H/(L - H)$	0.27
$(H - HS)/(L - H)$	0.53
$(L - LS)/(L - H)$	0.69
$(LS - HS)/(L - H)$	2.23

also been observed by [12] but at much higher pressures. In-beam studies with a gas ΔE detector in conjunction with a stopping solid-state detector were not done as they have been pursued in detail by several workers [15-19].

There are however certain limitations on the detector performance. For example, the charge induced due to moving electrons ($q_{ind}^{(-)}$) and positive ions ($q_{ind}^{(+)}$) is given by the Shockley-Ramo Theorem [3,20,21] as

$$q_{ind}^{(-)} = -\frac{e}{W} \int_0^d \frac{dE(z)}{dz} [\phi_w(d) - \phi_w(z)] dz \quad (3)$$

$$q_{ind}^{(+)} = -\frac{e}{W} \int_0^d \frac{dE(z)}{dz} [\phi_w(z) - \phi_w(0)] dz \quad (4)$$

where e is the electronic charge, W is the mean energy for ionization, $\frac{dE(z)}{dz}$ the stopping power of the incident particle in the gas and $\phi_w(z)$ is the weighting potential in the present case at any point z along the particle track, d being the anode-cathode separation. If the particle stops inside the detector active length the upper limit in the integrals should be replaced by the range of the particle.

The total induced charge is a result of the motion of all the ionizations that occur along the track between the cathode and anode. As can be seen from equations (3) and (4), in the electron sensitive operation [3] of the detector, the anode signal is not proportional to the energy deposited

by the particle (due to the z dependence of ϕ_w). This problem can be reduced if a Frisch Grid is placed between the cathode and anode. The weighting potential is now suppressed between the cathode and grid ($\phi_w = 0$ for $0 < z < b$) so that equation (3) reduces to

$$q_{ind}^{(-)} = -\frac{e}{W} \int_0^b \frac{dE(z)}{dz} [\phi_w(d) - \phi_w(z)] dz - \frac{e}{W} \int_b^d \frac{dE(z)}{dz} [\phi_w(d) - \phi_w(z)] dz \quad (5)$$

The proportionality to energy loss is thus ensured in the region between cathode and grid. However, the source of non-uniformity (second term of (5)) cannot be completely eliminated in an axial mode but can be reduced by keeping the separation between grid and anode small. In this work we have used a very simple electrode structure keeping the holes in the guard plates empty. The weighting potential for the present electrode configuration ($b/d = 0.5$) is calculated by using the formalism of ref [22] (subject to the boundary conditions in the present case) and depicted in fig.7. The weighting potential along the axis of the detector is plotted where the distortion in the region between the cathode and the guard plate due to the hole in the plate is maximum. This effect reduces as one moves away from the axis. The effect of a guard plate without a hole which entirely suppress ϕ_w between the cathode and grid is shown for comparison. In the practical case a transparent mesh has to be used. However use of additional mesh besides the anode may add to a background in the detector spectrum due to unwanted scattering of the incident particles [4]. Thus in an axial chamber the Frisch grid is not completely effective as in a transverse field chamber.

If however the Bragg-curve of the particle is approximately constant over the detector length, equations (3) reduces to

$$q_{ind}^{(-)} \approx -\frac{e}{W} S \int_0^d [1 - \phi_w(z)] dz \quad (6)$$

where S is the constant stopping power. The result of the integration will always be a function of d (i.e, independent of z) irrespective of the form of $\phi_w(z)$. Thus the measured signal will be proportional to the energy lost (Sd) by the particle in the detector active length. In the present work the Bragg-curve for a 6.12 MeV α particle and the ^{252}Cf fission fragments are almost constant over the cathode-anode gap (20 mm) and so the detector functions satisfactorily as a ΔE device.

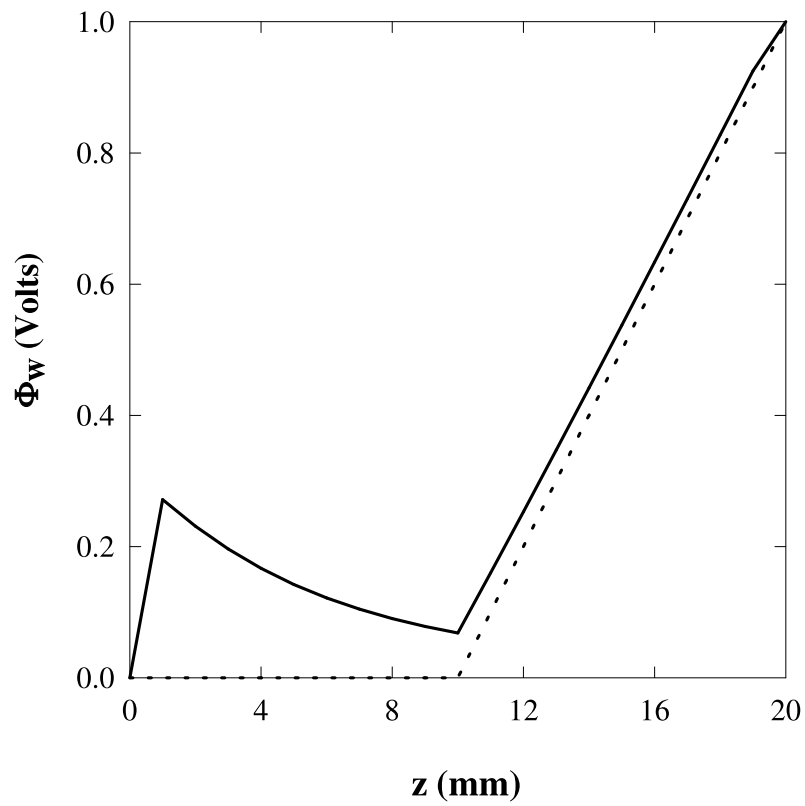


Figure 7: Plot of weighting potential ϕ_w in the present electrode geometry (solid line) along the axis of the detector. The dotted line represents the weighting potential for the case of guard plate with no hole.

4 Summary and conclusion

We have fabricated a gas ionization chamber working in the axial mode charge collection configuration using parallel plate geometry. The different parameters like the gas type and pressure, anode voltage and anode structure have been optimized. In particular the effect of anode structure has been studied. A mesh with parallel array of round wires was found to give better energy resolution. A higher transparency is found to give better resolution, although a larger fluctuation of the mesh voltage was associated with it. Therefore, a parallel array of $12.5 \mu\text{m}$ round gold plated wires will be used in future to get better resolution.

5 Acknowledgement

The author(S.A.) would like to thank Ms. S. Bhattacharyya, Prof. S. Saha, Mr. Dulal Ghosal, Mr. S. Chakraborty and SINP workshop for their help at different stages of this work.

References

- [1] W. Assmann, Ionization Chambers for Materials Analysis with Heavy Ion Beams, Nucl. Inst. Meth. Phys. Res. **B 64** (1992) 267-271.
- [2] Chinmay Basu, B.P. Das, Subinit Roy, P. Basu, H. Majumdar and, M.L. Chatterjee, Performance of a position sensitive low-pressure wire chamber (LPWC) having position readout from a separate sense wire plane: a critical analysis, Nucl. Inst. Meth. Phys. Res. **A 484** (2002) 407.
- [3] G.F. Knoll, *Radiation, Detection and Measurement*, 3rd edition, John Wiley & Sons, Inc (2000).
- [4] R.W. Zurmühle and L. Csihas, A $\Delta E - E$ Telescope with Very Large Solid Angle, Nucl. Inst. Meth. **203**(1982) 261-267.
- [5] S.K. Bandopadhyaya et al., An Axial Ionization Chamber for Heavy Ion Identification, Nucl. Inst. Meth. Phys. Res. **A 278** (1989) 467-469.
- [6] Rita B.J. Palmer, The Stopping Power of Hydrogen and Hydrocarbon Vapours for Alpha Particles over the Energy Range 1 to 8 MeV, Proc. Phys. Soc. **87** (1966) 681-688.

- [7] J. F. Ziegler et al, The Stopping Range of Ions in Solids Pergamon Press, New York, (1966)
- [8] S. Altieri et al., A compact solid-state detector for small angle particle tracking, Nucl. Inst. Meth. Phys. Res. **A 452** (2000) 185-191.
- [9] A. N. James, P.A. Butler, T.P. Morrison, J. Simpson K. A. Connell, The Response of an isobutane filled ion chamber to heavy ions, Nucl. Inst. Meth. **212** (1983) 545-553.
- [10] H.W. Fulbright, Ionization Chambers, Nucl. Inst. Meth. **162** (1979) 21-28.
- [11] F.H. Read, N.J. Bowring, P.D. Bullivant, and R.A. Ward, Penetration of Electrostatic Fields and Potentials Through Meshes, Grids, or Gauzes, Rev. Sc. Inst. **69** (1998) 2000.
- [12] N. N. Ajitanand, S.K. kataria, S.S. Kapoor and P.N. Rama Rao, A ΔE gas ionization chamber for fission fragments, Nucl. Inst. Meth. **103** (1972) 169-170.
- [13] H. Sann et al, A position sensitive ionization chamber, Nucl. Inst. Meth. **124** (1975) 509-519.
- [14] D.A. Sykess and S.J. Harris, Energy Stragglng of Fission Fragments in Thick Absorbers, Nucl. Inst. Meth. **97** (1971) 203-205.
- [15] C.E. Anderson, D.A. Bromoley, and M. Sachs, Simultaneous nuclide identification and energy measurement of nuclear reaction products, Nucl. Inst. Meth. **13** (1961) 238-243.
- [16] M. V. Sachs, C. Chasman, and D. A. Bromley, Heavy ion reaction product identification by measurement of dE/dx and E , Nucl. Inst. Meth. **41** (1966) 213-225.
- [17] A. Gamp, W. Bohne, P. Braun-Munzinger, and C. K. Gelbke, Complete identification of heavy ions by means of a time-of-flight spectrometer with ΔE ionization chamber Nucl. Inst. Meth. **120** (1974) 281-286.
- [18] J. Barrette, P. Braun-Munzinger, and C. K. Gelbke, $\Delta E - E$ telescope for the identification of heavy ions at low energies with good energy resolution and optimum ΔE resolution, Nucl. Inst. Meth. **126** (1975) 181-187.

- [19] F.S. Goulding and B.G. Harvey, Identification of Nuclear Particles, *Ann. Rev. Nucl. Sc.* **25** (1975) 167-240.
- [20] W. Shockley, Currents to Conductors Induced by a Moving Point Charge, *J. Appl. Phys.* **9** (1939) 635-636.
- [21] Zhong He, Review of the Shockley-Ramo theorem and its application in semiconductor gamma-ray detectors, *Nucl. Inst. Meth. Phys. Res. A* **463** (2001) 250-267.
- [22] J.D. Jackson, *Classical Electrodynamics*, 2nd edition, Wiley Eastern Limited, (1989) 121-126.